Inorganic Chemistry

Article

pubs.acs.org/IC

Observation of an Organic Acid Mediated Spin State Transition in a Co(II)−Schiff Base Complex: An EPR, HYSCORE, and DFT Study

Evi Vinck,[†] Emma Carter,[‡] Damien M. Murphy,*[,‡] and Sabine Van Doorslaer*[,†]

[†]Department of Physics, University of Antwerp, B-2610 Antwerp, Belgium

[‡]School of Chemistry, Cardiff University, Main Building, Park Place, Cardiff CF10 3AT, United Kingdom

Supporting Information

ABSTRACT: The interactions of a weak organic acid (acetic acid, HOAc) with a toluene solution of the Co^{II}−Schiff base type complex, (*R*,*R*′)-*N*,*N*′-bis(3,5-di-*tert*-butylsalicylidene)-1,2-cyclohexane-diamino Co^{II} (labeled [Co(**1**)]), was investigated using EPR, HYSCORE, and DFT computations. This activated [Co^{II}(**1**)] system is extremely important within the context of asymmetric catalysts (notably the hydrolytic kinetic resolution of epoxides) despite the lack of detailed structural information about the nature of the paramagnetic species present. Under anaerobic conditions, the LS [Co^{II}(**1**)] complex with a $|yz, {}^2A_2\rangle$ ground state is converted into a low-spin (LS) and a high-spin (HS) complex in the presence of the acid. The newly formed LS state is assigned to the coordinated [Co^{II}(**1**)]-(HOAc) complex, possessing a $|z^2, {}^2A_1\rangle$ ground state (species A; g_x = 2.42, g_y = 2.28, g_z = 2.02, A_x = 100, A_y = 120, A_z = 310 MHz). The newly formed HS state is assigned to an acetate coordinated [Co^{II}(**1**)]−(OAc^-) complex, possessing an $S = {}^3/_2$ spin ground state (species B, responsible for a broad EPR signal with $g \approx 4.6$). These spin ground states were confirmed with DFT calculations using the hybrid BP86 and B3LYP functionals. Under aerobic conditions, the LS and HS complexes (species A and B) are not observed; instead, a new HS complex (species C) is formed. This complex is tentatively assigned to a paramagnetic *superoxo* bridged dimer (AcO^-)[Co^{II}(**1**)···$O_2^-$$Co^{III}$(**1**)](HOAc), as distinct from the more common diamagnetic *peroxo* bridged dimers. Species C is characterized by a very broad HS EPR signal (g_x = 5.1, g_y = 3.9, g_z = 2.1) and is reversibly formed by oxygenation of the LS [Co^{II}(**1**)]−(HOAc) complex to the superoxo complex [Co^{III}(**1**)O_2^-](HOAc), which subsequently forms the association complex C by interaction with the HS [Co^{II}(**1**)](OAc^-) species. The LS and HS complexes were also identified using other organic acids (benzoic and propanoic acid). Thermal annealing−quenching experiments revealed the additional presence of [Co^{III}(**1**)O_2^-](HOAc) adducts, corroborating the presence of species C and the presence of diamagnetic dimer complexes in the solution, such as the EPR silent (HOAc)[Co^{III}(**1**)(O_2^{2-})Co^{III}(**1**)](HOAc). Overall, it appears that a facile interconversion of the [Co(**1**)] complex, possessing a LS ground state, occurs in the presence of acetic acid, producing both HS and LS Co^{II} states, prior to formation of the oxidized active form of the catalyst, [Co^{III}(**1**)](OAc^-).

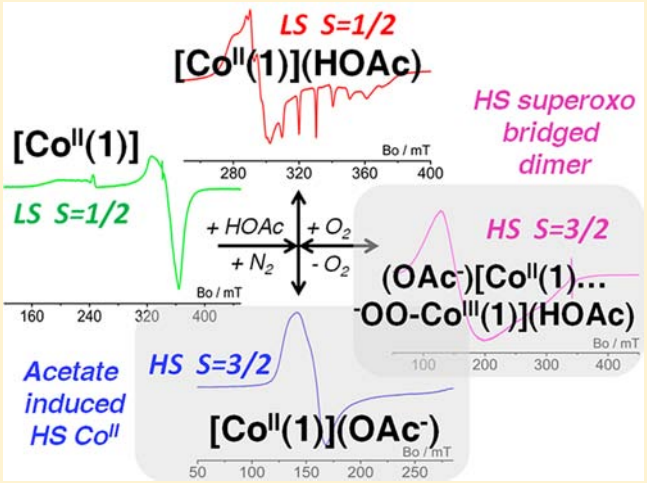

INTRODUCTION

Stereochemistry in chemical reactions is important in several branches of research, including the biological, agrochemical, and pharmaceutical sciences.[1] This importance originates from the fundamental prerequisite of chiral recognition in drug−receptor interactions, since most biological targets are chiral entities.[2] As a result, there is enormous demand to devise viable and practical methods for the preparation of chiral compounds, either through asymmetric synthesis or asymmetric catalysis.[3] In the specific case of asymmetric catalysis, chiral metal−salen complexes are currently among the most important class of synthetic ligand systems, particularly for the kinetic resolution of epoxides.[4] Early investigations into the challenging enantioselective epoxidation of unfunctionalized olefins by chiral (salen)Mn^{III} provided access to a range of epoxides with high levels of enantioselectivity.[5] Chiral salen complexes of Cr and Co catalyze the ring-opening of epoxides, and they are particularly efficient at promoting the hydrolytic kinetic resolution (HKR) of racemic epoxides. With these catalysts, epoxides with >99% enantiomeric excess (ee) can be obtained in high yields.[6] The most commonly employed catalyst is the acetate derivative, (salen)Co(OAc), formed by stirring the parent cobalt salen complex in acetic acid under air.[7]

Despite its widespread use, some structural aspects of the HKR reaction using Co−salen complexes remain unclear. The

Received: January 10, 2012
Published: July 25, 2012

   dx.doi.org/10.1021/ic300058p | *Inorg. Chem.* 2012, 51, 8014−8024

precatalyst is usually based on the *N,N′*-bis(3,5-di-*tert*-butylsalicylidene)-1,2-cyclohexane-diamino Co^{II} salen complex, [Co(**1**)]. As mentioned above, this Co^{II} complex is first activated by addition of a weak organic acid (such as acetic acid in toluene) while stirring under air. Although the kinetic aspects of this reaction mechanism have been clearly demonstrated,[8,9] the structural nature of all complexes existing in the activated catalyst, particularly the paramagnetic complexes, remains poorly understood. A recent NMR and quantum chemical investigation focused on the nature of the paramagnetic high-spin Co^{III} species in the reaction.[10] Furthermore, while the active form of the catalysts certainly contains Co^{III}, there appear to be some contradictory reports on the diamagnetic versus paramagnetic properties of the activated complex.[11,12] Therefore, we considered it very valuable and timely to instigate an in-depth characterization of specifically the paramagnetic species present in the activated Co^{II}–salen complex using advanced EPR techniques.

The catalyst is also recoverable *via* evaporation of the volatile reactants and products, and can be easily regenerated.[6] A number of recent studies have focused on the various factors influencing the recyclability of these Co^{III}–salen catalysts, in particular the progressive loss in activity with multiple recycles.[7,13−15] Three hypotheses have been suggested associated with the deactivation of the Co^{III}–salen–X catalyst (X = counterion), including (i) counterion exchange,[13,14] (ii) reduction of Co^{III} to Co^{II},[7,15,16] and (iii) salen ligand hydrolysis.[17] Interestingly, a well-known characteristic of the salen type ligand is the potential to form multinuclear complexes.[18−21] The potential role, if any, of such multinuclear (dimer) complexes in the chemistry of the HKR reaction has not been widely considered to date.

In order to bridge the gap in our understanding of the nature of the activated complex, we recently investigated the electronic structure of [Co(**1**)] using continuous wave (CW) and pulsed electron paramagnetic resonance (EPR), in combination with density functional theory (DFT) computations.[22,23] CW EPR revealed the formation of a low-spin (LS) Co^{II} complex and an unidentified high-spin (HS) species upon addition of acetic acid to [Co(**1**)] under an anaerobic (N_2) atmosphere. Under aerobic conditions (i.e., conditions analogous to the actual activation step of the catalyst), we furthermore identified the formation of a coordinated Co^{III}-bound phenoxyl radical, labeled $[Co^{III}(\mathbf{1}^{\bullet})(OAc)_n](OAc)_m$ ($n = m = 1$ or $n = 2$, $m = 0$).[23] In the current work, the nature of these HS and LS Co^{II} complexes, formed in the anaerobic and aerobic system following addition of different weak organic acids, will be further elucidated using CW EPR, HYSCORE (hyperfine sublevel correlation) spectroscopy, and DFT computations. We will reveal how different spin states of the Co^{II} center are accessed by coordination of the acid (HOAc) or base (OAc^-), and how these LS and HS complexes are unusually transformed into a novel superoxo bridged dimer.

METHODS

Sample Preparation. Commercially available (*R,R′*)-*N,N′*-bis(3,5-di-*tert*-butylsalicylidene)-1,2-cyclohexane-diamino Co^{II}, hereafter labeled [Co(**1**)] (see Scheme 1), was obtained from Sigma-Aldrich (CAS: 176763-62-5). For EPR analysis, the complex was dissolved in dried toluene. Concentrations of 10−80 mM were used for the CW and pulsed-EPR experiments. To investigate the interaction of the weak organic acids with [Co(**1**)], 10 equiv of acetic acid (CH_3COOH), benzoic acid (C_6H_5COOH), or propanoic acid (CH_3CH_2COOH) (all ex Sigma-Aldrich) was added to a toluene solution of (*R,R′*)-[Co(**1**)] (80 mM) directly under air or under anaerobic conditions. The anaerobic experiments were performed either in a GANUK GmbH glovebox under N_2 (<10 ppm O_2) or on a Schlenk line operating under an Ar atmosphere. ^{13}C-Labeled acetic acid (acetic acid-1-13C, ex Sigma Aldrich, 99 atom %^{13}C) was also used. In order to test the ability of axial ligand binding to the different complexes, pyridine (Fluka, puriss.) was sometimes added to the activated [Co^{II}(**1**)] system (see Results section for a detailed description).

Scheme 1. Proposed Structures of the LS Species A {[Co^{II}(1**)](HOAc)}, HS Species B {[Co^{II}(**1**)](OAc^-)}, and HS Species C {(OAc^-)[Co^{II}(**1**)···$O_2^-$$Co^{III}$(**1**)](HOAc)}, Illustrating the Transformations Occurring to [Co^{II}(**1**)] with Acetic Acid under *Anaerobic* and *Aerobic* Conditions[a]**

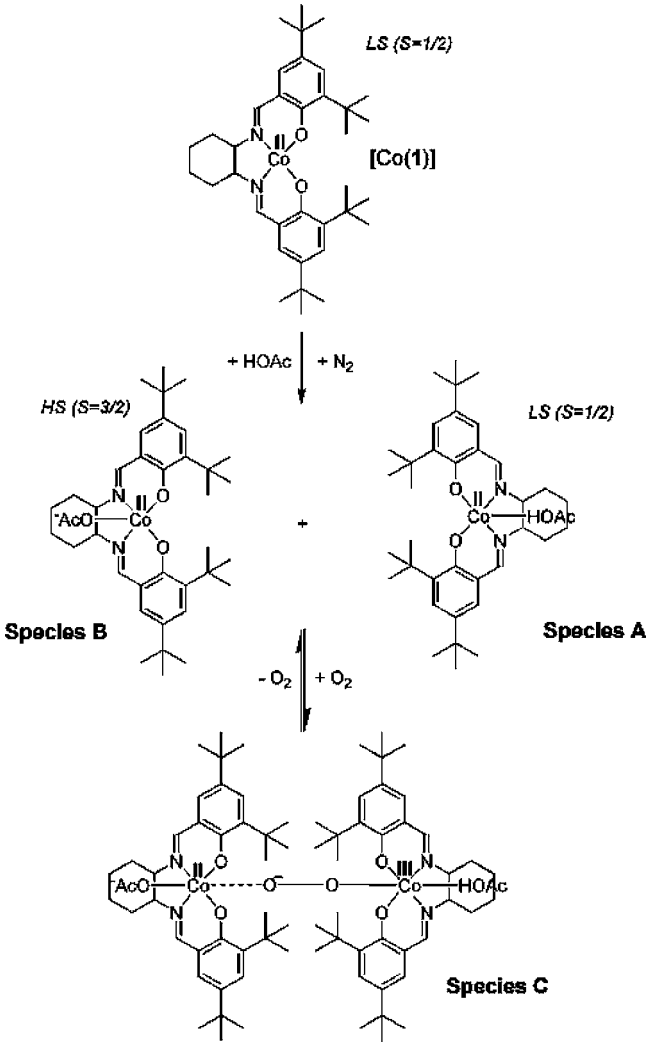

[a] The starting (*R,R′*)-*N,N′*-bis(3,5-di-*tert*-butylsalicylidene)-1,2-cyclohexane-diamino Co^{II} complex is labeled [Co(**1**)].

Spectroscopic Techniques. The X-band CW-EPR experiments were performed on a Bruker ESP300E spectrometer (microwave (mw) frequency 9.45 GHz) equipped with a gas-flow cryogenic system (Oxford, Inc.), allowing operation from room temperature down to 2.5 K. The magnetic field was measured with a Bruker ER035M NMR gaussmeter. The spectra were recorded at different temperatures in the 4−100 K range (see details in figure captions) using a microwave power of 2 mW, a modulation amplitude of 0.2 mT, and a modulation frequency of 100 kHz. Simulations of all CW EPR spectra were performed with the EasySpin program, a Matlab toolbox developed for EPR simulations[24] (www.easyspin.org).

dx.doi.org/10.1021/ic300058p | *Inorg. Chem.* 2012, 51, 8014−8024

Hyperfine sublevel correlation (HYSCORE) experiments[25] were carried out using the pulse sequence $\pi/2-\tau-\pi/2-t_1-\pi-t_2-\pi/2-\tau-$echo, with pulse lengths of $t_{\pi/2} = t_\pi = 16$ ns. Times t_1 and t_2 were varied from 96 to 5680 ns in steps of 16 ns. An eight-step phase cycle was used to eliminate unwanted echoes. The individual time traces were baseline corrected with a third-order polynomial, apodized with a Hamming window, and zero-filled. After 2D Fourier transformation, the absolute-value spectrum was calculated. The HYSCORE spectra were simulated using a GAMMA[26]-based program developed at the ETH Zurich.[27] The same sets of τ values as in the experiments were taken. For the simulation, ideal pulses were used with the same pulse lengths as in the experiment. The Euler angles α, β, and γ define an active rotation (right-hand) of the matrices and tensors with respect to the g principal axes system (i.e., rotation about the z axis over angle α, followed by rotation of angle β about the new y axis, with subsequent rotation about the new z axis over angle γ).

DFT Computations. Spin-unrestricted density functional computations were performed with the ORCA package[28−31] on different [Co(**1**)]-derived complexes modeling the acid activation. The outer tertiary butyl groups of the aromatic ring were replaced by methyl groups, in order to reduce the computation time ([Co(**1′**)], see details in text and in Supporting Information).

Computation of EPR Data. Geometry optimization was performed with the B3LYP functional, with an Ahlrich-TZV basis set[32] with pp polarization functions (TZVPP) (Ahlrich and coworkers, unpublished) for the cobalt ion, and Gaussian 6_31G basis functions[33,34] with polarization functions from the basis 6-311++G(d,p)[35] for the other atoms. For the calculation of the hyperfine principal values, basis sets with more flexibility in the core region were tried, i.e., the ORCA basis sets "CoreProp" (CP(PPP)) for the cobalt ion, and "EPRIII"[36] for the nitrogens and ^{13}C nuclei, and the TZVPP basis set for all other atoms. The basis sets are mentioned in the appropriate figure and table captions.

In order to account for solvent effects, some calculations were also performed with the conductor-like screening model (COSMO), that is implemented into ORCA.[37] The dielectric constant of the toluene (ε_1= 2.4 at 20 °C)−acetic acid (ε_2 = 6.2 at 20 °C) mixture was calculated using the formulas given in ref 38 yielding a constant of 2.5. Since the calculations, in which the solvent effects were taken into account, gave very similar results as the *in vacuo* calculations, they will not be given here.

Relative Energy Computations. In order to compute the relative energies of the LS ($S = {}^1/_2$) and HS ($S = {}^3/_2$) [Co(**1′**)](L)$^-$ and [Co(**1′**)](HL) complexes (L = OAc$^-$, OPr$^-$, or OBz$^-$), geometry optimizations were performed using the Becke−Perdew density functional BP86[39,41] together with the resolution of identity method.[42,43] The Ahlrich split-valence plus polarization (SVP) basis set was taken for all atoms except for the cobalt atom for which a more polarized triple-ζ valence (TZVPP) basis was used. The energy was converged to 1×10^{-8} hartree (Eh), and the convergence tolerances in the geometry optimization were 3×10^{-4} Eh/bohr for the gradient and 5×10^{-6} Eh for the total energy. No symmetry constraints were imposed during the geometry optimization. The COSMO model[37] was used assuming a toluene matrix. Separate geometry optimizations were also performed for [Co(**1′**)], acetate, and acetic acid in this matrix. Since recent work of Pietrzyk et al.[44] showed the immense influence of the functional on the relative energy of computed LS and HS Co^{II} complexes, single-point energy computations were performed both with the BP86 functional and with the B3LYP functional on the optimized structures.

RESULTS

The starting Co^{II} complex [Co^{II}(**1**)] is catalytically inactive for the HKR of epoxides. It must first be activated *via* a one-electron oxidation by aerobic oxidation using a mild Brønsted acid such as acetic acid (CH_3COOH, abbreviated hereafter to HOAc). This process produces the active form of the catalyst, thought to be [Co^{III}(**1**)]$^+$−(X) (X = counterion). To systematically unravel the nature of the paramagnetic species formed during this activation process, [Co^{II}(**1**)] was activated in different ways in the following study: (i) by addition of acetic acid to (*R*,*R′*)-[Co(**1**)] under *anaerobic* conditions, (ii) by subsequent addition of air/O_2 to step i, and finally (iii) by addition of acetic acid to (*R*,*R′*)-[Co(**1**)] directly under *aerobic* conditions.

Acetic Acid Addition to [Co(1)] under Anaerobic Conditions. The CW-EPR spectrum of (*R*,*R′*)-[Co(**1**)] dissolved in toluene is shown in Figure 1a. An identical

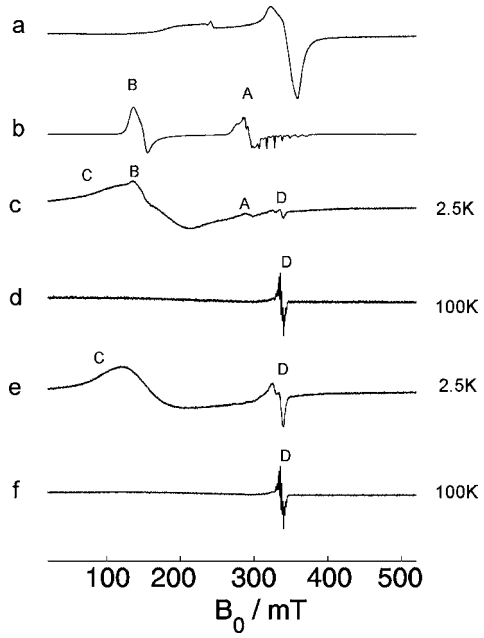

Figure 1. X-band CW-EPR spectra of a frozen toluene solution of (a) (*R*,*R′*)-[Co(**1**)] (recorded at 100 K) and (b) (*R*,*R′*)-[Co(**1**)] after addition of acetic acid (10 equiv) under a nitrogen atmosphere (recorded at 10 K). (c, d) X-band CW-EPR spectra of b after exposure to air (30 min) and recorded at (c) 2.5 K and (d) 100 K. (e, f) X-band CW-EPR spectra of a frozen toluene solution of (*R*,*R′*)-[Co(**1**)] after addition of acetic acid (10 equiv) under aerobic conditions (10 h, to highlight signal C) recorded at (e) 2.5 K and (f) 100 K.

spectrum was obtained using the opposite enantiomer, (*S*,*S′*)-[Co(**1**)] (not shown). The features of this EPR spectrum were discussed elsewhere by us,[22] and the spin Hamiltonian parameters (see Table 1) were shown to be typical of a LS Co^{II} center possessing a $|yz, {}^2A_2\rangle$ ground state.[45] Figure 1b shows the resulting CW-EPR spectrum of (*R*,*R′*)-[Co(**1**)] after addition of 10 equiv of acetic acid under anaerobic conditions (*via* step i as described above). Two new EPR signals are observed, due to the presence of new paramagnetic centers, hereafter labeled species A and B. Similar observations were also obtained after addition of different levels of acetic acid, ranging from 1 to 33 equiv (spectra not shown for brevity). The g and cobalt hyperfine values of species A are typical of a LS Co^{II} center and agree with those found for related Co^{II} salen-type complexes possessing a $|z^2, {}^2A_1\rangle$ ground state (see Table 1).[22] This signal is visible over a range of temperatures, from 10 to 60 K (Figure S1, Supporting Information, SI).

Since this $|z^2, {}^2A_1\rangle$ ground state is generally induced in Co^{II}−Schiff base complexes through axial ligation of a σ donor, acetic acid or acetate (HOAc/OAc$^-$) are the most likely σ donors responsible for signal A (Figure 1b). To confirm this, comparative HYSCORE experiments of (*R*,*R′*)-[Co(**1**)] after

dx.doi.org/10.1021/ic300058p | Inorg. Chem. 2012, 51, 8014−8024

Table 1. Experimental Principal g and Cobalt Hyperfine Values of the Species Obtained During Aerobic and Anaerobic Acetic Acid Activation of [Co^{II}(1)] Compared to Those Found for Related Co^{II} Systems

	g_x	g_y	g_z	$A_{x'}^{Co}$ (MHz)	$A_{y'}^{Co}$ (MHz)	$A_{z'}^{Co}$ (MHz)	ref
			Experimental				
[Co(**1**)][a]	3.21 (±0.03)	1.89 (±0.01)	1.98 (±0.01)	±400 (±25)	|A| < 80	±125 (±15)	22
species A[a] [Co(**1**)](HOAc)	2.420 (±0.010)	2.280 (±0.010)	2.020 (±0.005)	±100 (±15)	±120 (±15)	±310 (±10)	this work
species B [Co(**1**)](OAc^-)		g = 4.6 (±0.1)					this work
species C (OAc^-)[Co^{II}(**1**)···$O_2^-Co^{III}$(**1**)] (HOAc)	5.1 (±0.1)	3.9 (±0.2)	2.1 (±0.5)				this work
species D [Co^{III}(**1**$^•$)$(OAc)_n$]$(OAc^-)_m$	2.0060 (±0.0005)	2.0031 (±0.0004)	1.9943 (±0.0002)	17 (±2)	55 (±5)	14 (±2)	23
species E [Co^{III}(**1**)O_2^-]$(OAc^-)_{n=0,1}$	2.010 (±0.01)	1.990 (±0.005)	2.078 (±0.005)	70 (±5)	45 (±5)	20 (±20)	this work
Related Systems							
[Co(saphen)]THF[b]	2.514	2.256	2.017	±174	±97	±336	45
[Co(salen)]DMSO[c]	2.50	2.30	2.013	|A| < 186	|A| < 90	±357	45
[Co(salen)]py[d]	2.450	2.212	2.006	+ 133 $\|A^N\|$ = 40 MHz	+ 33	+ 271	71
[$Co^{II}(dmgH)_2$][e]	2.31	2.194	2.009	±70	±20	±328	72
Cobester[f]	2.447	2.447	1.990	±273	±273	±430	73
[Co^{III}(**1**)O_2^-]Py	2.006 (±0.010)	1.990 (±0.005)	2.075 (±0.005)	55 (±5)	20 (±5)	38 (±5)	23

[a]In toluene. [b]In 60% toluene, 40% tetrahydrofuran (THF), glass. [c]In dimethyl sulfoxide (DMSO), glass. [d]Single crystal. [e]In H_2O, dmgH = bis(dimethylglyoximato). [f]In toluene, Cobester = dicyano-heptamethylcobyrinate. Note: The g_x, g_y, and g_z axes of species A are situated along the x, y, and z molecular axes (see SI). The orientation of the cobalt hyperfine principal axes of species A is shown in the SI. The listed [Co(**1**)] complexes in the Table are of the (R,R') enantiomer. For species E and [Co^{III}(**1**)O_2^-]Py, the angle between the A_z and g_z axis is 60 ± 10°.

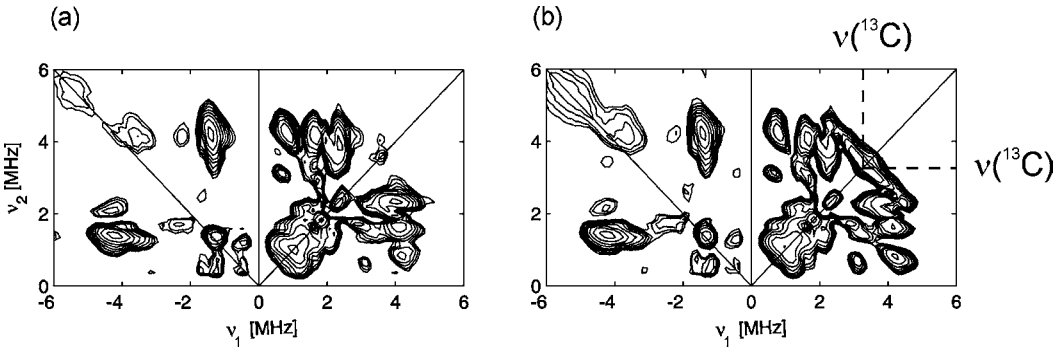

Figure 2. X-band HYSCORE spectra recorded at a magnetic-field position corresponding with $g \sim 2.27$ of (a) a frozen toluene solution of (R,R')-[Co(**1**)] after addition of 10 equiv of acetic acid under nitrogen atmosphere, and (b) a frozen toluene solution of (R,R')-[Co(**1**)] after addition of 10 equiv of ^{13}C-labeled acetic acid under nitrogen atmosphere. The spectra were recorded at 4 K and with a τ value of 176 ns.

Table 2. Nitrogen Principal Hyperfine and Nuclear-Quadrupole Values, Obtained from Simulations of the HYSCORE Spectra of Species A {[Co(1)](HOAc)} Compared to Those Found for Related Systems

	$\|A_1^N\|$ (MHz)	$\|A_2^N\|$ (MHz)	$\|A_3^N\|$ (MHz)	$\|a_{iso}^N\|$ (MHz)	P_1 (MHz)	P_2 (MHz)	P_3 (MHz)	ref
species A[a]	1.5 (±0.3)	2.0 (±0.3)	1.5 (±0.3)	2.0	−0.50 (±0.10)	−0.75 (±0.10)	1.25 (±0.20)	
	α_A, β_A, γ_A = $n45°$[b] (±10°), 0° (±30°), 0° (±10°)				α_P, β_P, γ_P = $n45°$[b] (±20°), 90° (±30°), 0° (±20°)			
$Co^{II}(dmgH)_2$[c]	2.53	1.90	1.90	2.11	−0.26	−1.45	1.70	72
Cobester[c]	3.2	2.4	2.7	2.8	−0.02	−0.83	0.85	73

[a]Toluene solution. [b]n = 1, 3. [c]In methanol. Note: The orientation of the nitrogen nuclear-quadrupole and hyperfine tensor is shown in SI. The [Co(**1**)] complex is of the (R,R') enantiomer.

addition of unlabeled and ^{13}C-labeled acetic acid were performed (Figure 2). An additional HYSCORE ridge becomes visible in the spectra in the presence of ^{13}C-labeled acetic acid (Figure 2). This ridge originates from the interaction with a ^{13}C nucleus and could be simulated using the principal hyperfine values [2 ± 0.2, −1 ± 0.4, −1 ± 0.4] MHz (simulation of the ^{14}N and ^{13}C contributions are shown in Figure S2, SI). In a simple point-dipolar approximation,[46] this ^{13}C hyperfine interaction corresponds to a Co−^{13}C distance of 0.28 ± 0.02 nm, proving the coordination of either acetic acid or acetate to [Co^{II}(**1**)]. The principal hyperfine and nuclear-quadrupole values of the ^{14}N nuclei (obtained from the simulation of the HYSCORE spectra) are listed in Table 2. HYSCORE experiments of [Co^{II}(**1**)] containing selectively deuterated acetic acid (CH_3COOD) were also performed, in an attempt to discriminate between coordinated acetate versus coordinated acid. Unfortunately, owing to the predicted small magnitude of the ^{2}H interaction for [Co^{II}(**1**)](CH_3COOD), coupled with the background ^{2}H signal from uncoordinated CH_3COOD, we

dx.doi.org/10.1021/ic300058p | Inorg. Chem. 2012, 51, 8014−8024

were unable to conclusively demonstrate the coordination of the acid for species A in this experiment.

The second signal, centered around $g = 4.6 \pm 0.1$ in Figure 1b (species B), is characteristic of a HS Co^{II} center ($S = {}^3/_2$). The intensity of this signal is rapidly lost at higher temperatures, and is virtually absent at $T = 60$ K (see Figure S1, SI). This species was found to be stable under anaerobic conditions and was already observed even when lower amounts of acetic acid were used (down to 1 equiv); this implies that formation of species B is not simply due to the 10-fold excess of acetic acid used in the current activation study. It should be noted that acetic acid addition to [Co(**1**)] under these anaerobic conditions did not lead to any perceptible change in color (the solution retained an orange-red appearance throughout, analogous to the starting solution of [Co(**1**)] dissolved in toluene). A dark brown coloration was, however, observed following aerobic addition of acetic acid (*vide infra*).

To gain further insights into the origin of species B, an additional experiment was performed using tertrabutylammoniumacetate (TBAA). Owing to the insolubility of certain acetates in toluene, such as NaOAc, the organic soluble TBAA was used instead as a simple source of OAc^- in order to generate [Co^{II}(**1**)](OAc^-) for EPR analysis. Although the dissociation of TBAA in toluene was small, nevertheless, the resulting EPR spectrum contained the characteristic signal of species B along with the signal of the residual, uncoordinated [Co^{II}(**1**)] complex (Figure S3, SI). There was no evidence of species A in these EPR spectra, suggesting that species B should be assigned to the HS [Co^{II}(**1**)](OAc^-) complex, while species A must then be considered as arising from the [Co^{II}(**1**)]·(HOAc) complex.

Acetic Acid Activation of [Co(1)] under Aerobic Conditions. The CW-EPR spectrum shown in Figure 1b changes drastically after exposure of the sample to air or O_2 for ~30 min *via* step ii (see Figure 1c,d, recorded at 2.5 and 100 K, respectively). Similar CW-EPR spectra were also observed when acetic acid was added directly to a toluene solution of (*R*,*R*′)-[Co(**1**)] under air for 30 min (i.e., via step iii). Two new species can be discerned in these spectra. At 2.5 K, an EPR signal (hereafter labeled C) of a HS Co^{II} center is observed with effective principal *g* values of $g_x = 5.1 \pm 0.2$, $g_y = 3.9 \pm 0.2$, $g_z = 2.1 \pm 0.5$ (Figure 1c,e). The CW-EPR spectra shown in Figure 1c,e were also found to depend strongly on the exposure time to air at room temperature (Figure S4, SI) as A and B signals disappear and are replaced by the signal assigned to species C. The solution develops a brown coloration during this time. The contribution of species C then increases with time, and further HS Co^{II} species are formed after long (>24 h) air exposure (Figure S4, SI). The difference between the HS signals B and C indicates that the acid-mediated change of (*R*,*R*′)-[Co(**1**)] is influenced by the presence of O_2 or that O_2 can act as a ligand to the newly formed complex.

The additional signal in the aerobically activated system, labeled species D, is more clearly observed at relatively higher temperatures (100 K; Figure 1d,f). At 2.5 K, this signal is strongly saturated under the measuring conditions ideal for observation of species C. The nature of species D has recently been discussed in detail by us[23] and was assigned to a coordinated Co^{III}-bound phenoxyl radical, labeled [Co^{III}(**1**$^{\bullet}$)·$(OAc)_n$]$(OAc)_m$ ($n = m = 1$ or $n = 2$, $m = 0$). This unusual ligand based radical species was present in relatively small amounts in the activated system.[23]

Acid Activation of [Co(1)] with Benzoic and Propanoic Acid. The identity of the counterion is known to greatly influence the reactivity, enantioselectivity, and catalyst lifetimes of [Co(**1**)] in the HKR reaction.[47] Although the acetate adduct of [Co^{III}(**1**)], formed by aerobic acetic acid addition, has been the most widely used catalyst to date, beneficial effects of other counterions such as OH, Cl, OBz, OPh, OTs, and SbF_6 have been noted.[7,11,47] We therefore decided to examine the influence of other weak organic acids, such as benzoic acid (C_6H_5COOH, abbreviated HOBz) and propanoic acid (CH_3CH_2COOH, abbreviated HOPr) on the EPR spectra of [Co^{II}(**1**)] under anaerobic and aerobic conditions (Figure 3a,b and Figures S5 and S6, SI). For completeness, the CW-EPR spectrum of [Co(**1**)] containing acetic acid is also shown in Figure 3c.

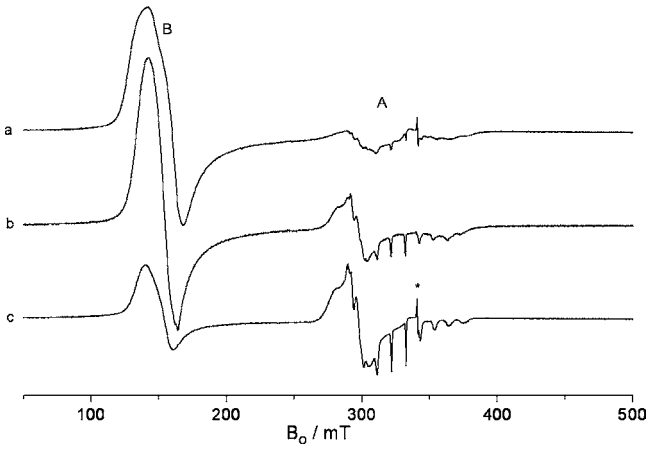

Figure 3. X-band CW-EPR spectra (10 K) of a frozen toluene solution of (*R*,*R*′)-[Co^{II}(**1**)] after addition of (a) benzoic acid (HOBz), (b) propanoic acid (HOPr), and (c) acetic acid (HOAc). * = cavity artifact. A 10 equiv portion of organic acid was added in each case.

The CW-EPR spectrum of (*R*,*R*′)-[Co(**1**)] recorded after addition of HOBz (10 equiv) under anaerobic conditions is shown in Figure 3a. Following anaerobic addition of the acid, the color of the solution progressively changed from orange-red to dark brown over a 30 min period. It should be recalled that no color change occurred using HOAc under identical anaerobic conditions. A strong HS Co^{II} signal was observed (B-type species), while a much weaker A-type LS Co^{II} signal was also seen (Figure 3a). Exposure of this sample to molecular oxygen (~30 min at room temperature) resulted in the loss of both A- and B-type signals and the appearance of a C-type signal (Figure S5, SI), similar to the acetic acid case (Figure 1), although the intensity of the C-type signal appeared lower in the HOBz case.

A similar series of observations were noted following addition of HOPr (10 equiv) to an anaerobic toluene solution of [Co(**1**)]. The resulting CW-EPR spectrum is shown in Figure 3b. Once again, a strong B-type signal was observed relative to the A-type signal. The intensity of this B-type signal diminished significantly at higher temperatures.

It should be noted that, upon lowering the temperature to 4 K, a second A-type signal was also observed after anaerobic addition of HOPr (Figure S5, SI). While the EPR parameters of the "high-temperature" A-type signal (at 60 K, $g_x = 2.430$, $g_y = 2.337$, $g_z = 2.089$, $A_x = 90$, $A_y = 17$, $A_z = 300$ MHz) are similar to those observed for signal A observed after acetic acid

dx.doi.org/10.1021/ic300058p | *Inorg. Chem.* 2012, 51, 8014−8024

addition, a second "low-temperature" A-type signal can also be detected at 4 K with somewhat different parameters (g_x = 2.430, g_y = 2.350, g_z = 2.062, A_x = 90, A_y = 17, A_z = 285 MHz). Similar spectral differences have been observed for mono- and bis-ligated Co^{II} porphyrin complexes,[48] indicating that the difference between the two A-type complexes (Figure S5, SI) lies in the number of axially coordinated propanoic acid or propanoate ligands. The equilibrium constant for binding a second axial substrate to a square planar Co^{II} complex is expected to be much less compared to the binding constant for a single axial ligand; hence, very low temperatures are required to form the bis-ligated complex. Furthermore, since the acid is in excess and therefore surrounds the complex, only a very small change in distance is required to effectively bind the second axial substrate at low temperatures. On the basis of the above results obtained using TBAA, where species A could be assigned to $[Co^{II}(\mathbf{1})](HOAc)$, the A-type signals observed with propanoic acid may be assigned to $[Co^{II}(\mathbf{1})](HOPr)_{n=1,2}$.

Upon oxygen exposure, a C-type signal also emerged in the spectrum (Figure S5, SI). These results reveal that similar types of LS and HS Co^{II} states (A-, B-, and C-type species) can also be formed in the presence of benzoic or propanoic acids. Although it is difficult to accurately quantify the abundances of the HS versus LS cobalt species based on these EPR spectra (due to differences in the relaxation times), it appears nevertheless that the relative intensities of signals A and B are quite different depending on the acid used (Figure 3).

Computational DFT Analysis of the HS and LS Co^{II} Complexes. A characteristic feature of Co^{II} complexes with the $3d^7$ electron configuration is the existence of a LS doublet ground state ($S = {}^1/_2$) or a HS quartet ground state ($S = {}^3/_2$). Pietrzyk et al.[44] recently discussed the computational approaches necessary to investigate which spin state exists in $[Co^{II}(acac)_2]$ as a function of ligand conformations. Unlike $[Co^{II}(acac)_2]$, $[Co^{II}(\mathbf{1})]$ does not possess large conformational flexibility, due to the rigid tetradentate binding motif of the salen ligand. Any observed change in the spin ground state can therefore only be induced by binding axial ligands, such as acetic acid or acetate, in the noncoordinating dry toluene solvent.

The optimized geometries for $[Co(\mathbf{1}')](HOAc)$ and $[Co(\mathbf{1}')](OAc^-)$, both in the LS and HS configurations, were therefore calculated. For $[Co(\mathbf{1}')](HOAc)$, binding of HOAc to the cobalt *via* the C═O or OH moiety were both considered, but only the former led to stable bound structures. The structures of both the HS and LS $[Co(\mathbf{1}')](HOAc)$ and $[Co(\mathbf{1}')](OAc^-)$ complexes are shown in Figure S7 (SI). For $[Co(\mathbf{1}')](HOAc)$, very little difference was seen in the Co—O bond lengths and O—Co—N bond angles between the doublet and quartet states (Table S1, SI). By comparison, appreciable differences were noted in the Co—O bond lengths and O—Co—N bond angles of $[Co(\mathbf{1}')](OAc^-)$ between the HS and LS states, such that the HS state was more asymmetrically distorted. The energy differences between the two spin states were calculated using either a GGA (generalized gradient approximation) functional (BP86) or a hybrid functional (B3LYP). The results obtained with the two functionals differ significantly (Table 3).

While both functionals predicted that LS $[Co(\mathbf{1}')](HOAc)$ is more stable than HS $[Co(\mathbf{1}')](HOAc)$, calculations using the BP86 functional suggested that formation of the $[Co(\mathbf{1}')](HOAc)$ is actually ill-favored (i.e., the sum of the energies of $[Co(\mathbf{1}')]$ and HOAc is lower than that of the complex). The latter functional contrasts the findings with the B3LYP, which showed that complexation leads to a stabilization. Both functionals showed that the formation of the $[Co(\mathbf{1})](OAc^-)$ complex is highly favored, but that addition of a second acetate ligand is ill-favored. While the BP86 functional suggested a doublet ground state for $[Co(\mathbf{1}')](OAc^-)$, a quartet ground state was predicted using the B3LYP functional (6.6 kcal mol^{-1} more stable than the corresponding doublet ground state). GGA functionals, such as BP86, are known to disfavor HS states, while the hybrid functional B3LYP disfavors LS states due to the large (20%) Hartree—Fock exchange.[49,50] In agreement with this, the experimentally observed $S = {}^3/_2$ ground state for tetrahedrally distorted $[Co(acac)_2]$ could be predicted with the B3LYP functional but not with GGA functionals.[44] Our current findings also reflect these known inaccuracies of the functionals in predicting spin states. Nevertheless, a number of important conclusions can be drawn from the DFT based data presented in Table 3: (i) axial ligation of HOAc is unlikely to induce a HS Co^{II} complex, since both functionals predicted the LS form to be more stable relative to the HS form; (ii) while it is unclear whether HOAc ligation leads to an energetically more favorable complex, ligation of OAc^- is certainly highly preferred; (iii) HS Co^{II} formation, induced by OAc^- ligation, is not unlikely (B3LYP result); and (iv) since the correct energy situation may be in-between the BP86 and B3LYP results, it is very probable that the doublet and quartet state of $[Co(\mathbf{1}')](OAc^-)$ are close in energy and may even coexist. These computational results thus indicate that the "high-temperature" A-type species observed with EPR can be assigned either to the LS $[Co(\mathbf{1}')](HOAc)$ or $[Co(\mathbf{1}')](OAc^-)$ complex (however, on the basis of the experimental evidence presented earlier, the former $[Co(\mathbf{1}')](HOAc)$ species is most likely), while the B-type species most likely agree with the quartet $[Co(\mathbf{1}')](OAc^-)$ complex (as is also confirmed by the above-mentioned experimental results).

As stated earlier, a number of other counterions have a noted beneficial effect in the HKR reaction with $[Co(\mathbf{1})]$. We therefore also sought to investigate the relative energies of the HS and LS states for $[Co(\mathbf{1}')]$ in the presence of water (i.e., H_2O/OH^-) and propanoic acid ($HOPr/OPr^-$). The main

Table 3. Relative Energies for Different Axial Donors in the $[Co(\mathbf{1}')]$ Complex Compared to the Sum of the Energy of the Individual Molecules[a]

		ΔE/kcal mol^{-1}	
	S	BP86	B3LYP
$[Co(\mathbf{1}')](OH^-)$	${}^1/_2$, ${}^3/_2$	0.0, 4.70	12.54, 0.0
$[Co(\mathbf{1}')] + OH^-$	${}^1/_2 + 0$	59.94	66.07
$[Co(\mathbf{1}')](H_2O)$	${}^1/_2$, ${}^3/_2$	0.0, 14.8	0.0, 6.31
$[Co(\mathbf{1}')] + H_2O$	${}^1/_2 + 0$	1.26	6.17
$[Co(\mathbf{1}')](OAc^-)$	${}^1/_2$, ${}^3/_2$	0.0, 9.47	6.6, 0.0
$[Co(\mathbf{1}')] + OAc^-$	${}^1/_2 + 0$	20.60	28.71
$[Co(\mathbf{1}')](HOAc)$	${}^1/_2$, ${}^3/_2$	0.55, 16.18	0.0, 3.01
$[Co(\mathbf{1}')] + HOAc$	${}^1/_2 + 0$	0.0	5.3
$[Co(\mathbf{1}')](OPr^-)$	${}^1/_2$ 3/2	0.0 8.43	7.70 0.0
$[Co(\mathbf{1}')] + OPr^-$	${}^1/_2 + 0$	15.07	24.55
$[Co(\mathbf{1}')](HOPr)$	${}^1/_2$, ${}^3/_2$	1.96, 16.01	0.0, 1.17
$[Co(\mathbf{1}')] + HOPr$	${}^1/_2 + 0$	0.0	3.67
$[Co(\mathbf{1}')](OAc^-)_2$	${}^1/_2$, ${}^3/_2$	17.95, 30.52	24.58, 21.01
$[Co(\mathbf{1}')](OAc^-) + OAc^-$	${}^1/_2 + 0$, ${}^3/_2 + 0$	0.0, 9.47	6.60, 0.0

[a]For a given density functional, the energy of the most stable state is set to zero.

dx.doi.org/10.1021/ic300058p | *Inorg. Chem.* 2012, 51, 8014−8024

aspects of the optimized geometries are summarized in Table S1 (SI). Similar to the above results obtained for coordinated HOAc/OAc$^-$, ligation of [Co(**1**′)] with the anions OH$^-$ or OPr$^-$ was also found to produce a quartet ground state using the B3LYP functional, while H_2O or HOPr coordination resulted exclusively in a doublet ground state (Table 3). It therefore appears generic that coordination of the anions (under the adopted experimental anaerobic conditions) can afford the HS state.

Furthermore, DFT computations were also performed to estimate the spin Hamiltonian parameters for LS [Co(**1**)]-(HOAc). These computations show that the LS complex, bearing coordinated HOAc, agrees with a $|z^2, {}^2A_1\rangle$ ground state (Figure S8, SI). Table 4 shows the comparison between the main experimentally accessible parameters and the computed values. None of the computed parameters match exactly with the experimental values, in agreement with the fact that current state-of-the-art DFT does not allow an exact quantitative prediction of the EPR parameters for Co^{II} complexes.[50] In particular, the isotropic part of the hyperfine tensors is strongly overestimated, while the anisotropic part is still reasonably well reproduced. Our earlier work on [Co(**1**)][22] revealed that the DFT-computed hyperfine values vary strongly with the choice of the basis sets, making it hard to gain accurate quantitative data other than differences in the general trend.

Table 4. Comparison between the Experimentally Observed EPR Parameters of Species A and the DFT Computed Values for [Co(1′)](HOAc)[a]

	[Co(**1**′)](HOAc) (DFT)	species A (EPR)
g	[2.37, 2.24, 2.01]	[2.42, 2.28, 2.02]
$\mathbf{A}^{Co}$ /MHz	[-19, 51, 537]	±[100, 120, 310]
$\mathbf{A}^{N}$ /MHz	[-4.5, −5.0, −5.5]	
		[−1.5, −2, −1.5]
	[-4.2, −4.5, −4.9]	
$\mathbf{A}^{C}$ /MHz	[5.2, 3.6, 2.4]	[2, −1, −1]

[a] $\mathbf{A}^{Co}$, $\mathbf{A}^{N}$, and $\mathbf{A}^{C}$ are the principal values of the hyperfine tensors of the central ^{59}Co nucleus, the ^{14}N nuclei of (**1**′), and the closest carbon of the HOAc ligand, respectively.

Evidence for Existence of Diamagnetic Species. It is entirely feasible that diamagnetic species are also generated following HOAc addition to [Co(**1**)]. Indeed, the oxidation of Co^{II}−Shiff base complexes to diamagnetic peroxo bridged dimer complexes is well known.[51] Although it is difficult to accurately determine the spin concentrations from the CW-EPR spectra (due to the mixture of HS and LS species with strongly different relaxation properties, as mentioned above), the overall EPR signal intensity of [Co(**1**)] (Figure 1a) appears to decrease following acetic acid addition under O_2/air (Figure 1c,d or Figure 1e,f) suggesting the formation of diamagnetic species. This EPR observation was also confirmed by UV−vis absorption spectroscopy, which is sufficiently sensitive to characterize various Co$^{II/III}$ species[52] in the activated system. Upon aerobic acid addition, the solution color changes from orange-red (for the nonactivated (*R*,*R*′)-[Co(**1**)]) to brown (for the activated (*R*,*R*′)-[Co(**1**)]). The resulting UV−vis absorption spectra (Figure S9, SI) are typical for Co^{III} species.[15] However, Co^{II} macrocyclic compounds are known to form dimeric complexes under air (*via* linkage of two Co^{II} complexes through a bridging peroxo O_2^{2-} group).[53] These resulting compounds are also diamagnetic (effectively [Co^{III}−O_2^{2-}−Co^{III}] dimers), and display similar UV−vis spectra as for the Co^{III} species reported here. In order to test whether these dimeric diamagnetic species could be present in the activated [Co(**1**)] solution, a series of additional experiments were performed (*vide infra*).

First, a toluene solution of (*R*,*R*′)-[Co^{II}(**1**)], originally activated with acetic acid under air (*via* step iii), was flushed with N_2 for 4 h. The sample was subsequently frozen, and the corresponding CW-EPR spectrum was measured (Figure 4b).

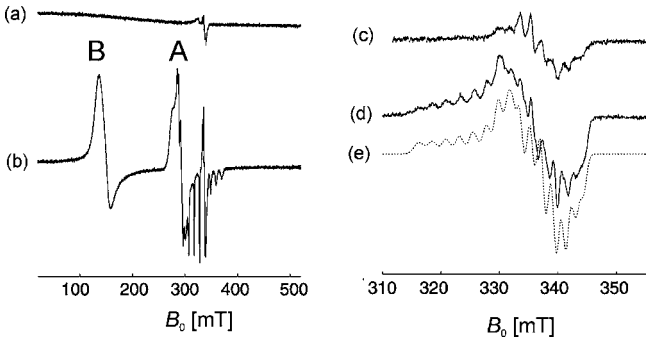

Figure 4. X-band CW-EPR spectra of (a) (*R*,*R*′)-[Co^{II}(**1**)] after addition of acetic acid (10 equiv) under air, and (b) subsequent flushing under N_2 during 4 h. (c, d) (*R*,*R*′)-[Co^{II}(**1**)] after addition of acetic acid (10 equiv) under air before (c) and after (d) heating to ∼70 °C and subsequent freeze- quenching. (e) Simulation of part d. All experimental spectra are recorded at 30 K (hence species C is not visible in part a).

The spectrum of the system activated under aerobic conditions is also shown for comparison in Figure 4a. Figure 4b contains two signals characteristic of the LS acetic acid ligated (*R*,*R*′)-[Co^{II}(**1**)] complex (species A) and the HS acetate ligated Co^{II} center (species B), identical to those previously reported in Figure 1b. This important experimental observation indicates the involvement of O_2 as a bridging ligand between the cobalt complexes (i.e., formation of a bridging superoxo or peroxo linkage, as discussed later). Interestingly, this reversibility was not observed with benzoic acid or propanoic acid.

Second, the acetic acid and air activated (*R*,*R*′)-[Co(**1**)] solution was heated to a temperature of ∼70 °C for 1 min and then immediately quenched in liquid nitrogen. Figure 4c,d shows an expanded part of the CW-EPR spectra taken before and after this heating/quenching cycle, respectively. The EPR intensity of the quenched spectrum (Figure 4d) increases by a factor of ∼3−4 and can be considered the sum of the original spectrum (Figure 4c containing species D, due to the coordinated phenoxyl radical[23]) plus a new component (species E), characteristic of an oxygenated Co^{II} species (i.e., (*R*,*R*′)-[Co^{III}(**1**)O_2^-], Figure 4d). Under these oxidative circumstances, it is of course impossible to form an oxygenated (*R*,*R*′)-[Co(**1**)] species starting only from an (*R*,*R*′)-[Co^{III}(**1**)]$^+$ complex (or from species D). Thus, the observation of the superoxo complex after heating can be explained by the presence of dioxygen-bridged dimers, such as the diamagnetic Co^{III}−O_2^{2-}−Co^{III} dimers, that decompose at elevated temperature. Rapid quench freezing traps some of the oxygenated (*R*,*R*′)-[Co(**1**)] complexes that are formed in this way (Figure 4d).

For comparison purposes, the CW EPR spectrum of a pyridine-ligated superoxo cobalt^{III} complex was also measured, (*R*,*R*′)-[Co^{III}(**1**)PyO_2^-]. The principal *g* and cobalt hyperfine

dx.doi.org/10.1021/ic300058p | *Inorg. Chem.* 2012, 51, 8014−8024

values for this latter species are actually slightly different compared to those observed for the pure oxygenated superoxo complex (*R*,*R*′)-[Co^{III}(**1**)O_2^-] (see Table 1). These two sets of values can be compared with the reported parameters for five- and six-coordinated oxygenated cobester superoxo complexes[54] and many other cobalt superoxo complexes.[55−58] This analysis suggests that the oxygenated (*R*,*R*′)-[Co(**1**)] superoxo species (species E), which is formed after heating the activated catalyst solution, can either be described as a five-coordinate complex or alternatively possess a weakly bound sixth ligand, such as acetic acid (Table 1).

DISCUSSION

Nature of Species A {LS [Co^{II}(1)](HOAc)} and Species B {HS [Co^{II}(1)](OAc$^-$)}. The EPR spectrum of [Co^{II}(**1**)] dissolved in toluene was shown in Figure 1a; the detailed spectroscopic features of this spectrum were described elsewhere.[22] Addition of acetic acid (HOAc) to the toluene solution of [Co^{II}(**1**)] under *anaerobic* conditions leads to the formation of two new paramagnetic species A and B (Figure 1b).

The *g* and ^{Co}A values for species A (Table 1) indicate the presence of a LS Co^{II} complex possessing a $|z^2, {}^2A_1\rangle$ ground state. This state is induced through axial ligation of a σ donor, as occurs in a range of related Co^{II}−salen complexes (see Table 1 and references therein). The coordination of either HOAc or OAc$^-$ was confirmed experimentally using ^{13}C-labeled acetic acid (HYSCORE spectrum shown in Figure 2). The observation of two A-type centers in anaerobic [Co(**1**)]/HOPr mixtures with parameters typical for axial mono- and bis-ligation of the σ donor suggests that species A is monoligated in the acetic acid case (see Figure S5, SI, which clearly shows the temperature induced transformation between the mono- and bis-ligated adducts).

Theoretical calculations, using the B3LYP and BP86 functionals, indicated that this doublet ground state can arise through coordination of the acid (HOAc), but that formation of LS [Co(**1**)](OAc$^-$) as well as a HS [Co(**1**)](OAc$^-$) complex cannot be fully ruled out. To experimentally ascertain which complex is responsible for species A or B, an organic acetate (TBAA) was added to [Co(**1**)] to generate [Co^{II}(**1**)](OAc$^-$). Only species B was observed by EPR in these experiments (Figure S3, SI), indicating that LS [Co(**1**)](OAc$^-$) is not accessible in our experiments and therefore species A must be assigned to LS [Co(**1**)](HOAc). Hence, formation of species A can be considered to result from the binding of acetic acid to [Co(**1**)]:

$$[Co^{II}(\mathbf{1})] + HOAc \rightarrow [Co^{II}(\mathbf{1})](HOAc) \quad \text{species A} \tag{1}$$

The second observed signal in Figure 1b, formed under *anaerobic* conditions, was assigned to a HS Co^{II} center (species B). The spin Hamiltonian parameters of species B bear all the hallmarks of a HS ($S = {}^3/_2$) Co^{II} center ($g = 4.6 \pm 0.1$), and DFT indicates that this quartet spin state originates from coordination of the acetate anion to [Co^{II}(**1**)], forming the HS [Co^{II}(**1**)](OAc$^-$) complex. This was also confirmed experimentally using TBAA and [Co^{II}(**1**)]:

$$[Co^{II}(\mathbf{1})] + HOAc \rightarrow [Co^{II}(\mathbf{1})](OAc^-) + H^+ \quad \text{species B} \tag{2}$$

In the operating HKR catalytic system, the diamagnetic [Co^{III}(**1**)](OAc$^-$) complex is regarded as the active species, responsible for binding either the electrophile or nucleophile in a reaction that is known to be second order with respect to the catalyst.[9] Since species B may be considered as the reduced form of [Co^{III}(**1**)](OAc$^-$), this could imply that acetic acid activation of [Co^{II}(**1**)] involves not only a change in oxidation state (from Co^{II} to Co^{III}) but also a change in spin state (from LS $S = {}^1/_2$ [Co^{II}(**1**)] to HS $S = {}^3/_2$ [Co^{II}(**1**)](OAc$^-$) and eventually to [Co^{III}(**1**)](OAc$^-$)). The exact spin state of cobalt in [Co^{III}(**1**)](OAc$^-$) was the subject of a recent combined NMR and quantum chemical study,[10] which revealed how Co^{III} can easily interchange between an LS hexacoordinated state in the [Co^{III}(**1**)](OAc$^-$)(THF) complex to a HS pentacoordinated state for the [Co^{III}(**1**)](OAc$^-$) complex; this spin change was dependent on the axial ligands, solvent, and temperature.[10] Hence, the $Co^{II} \rightarrow Co^{III}$ oxidation may be facilitated if both cobalt centers are already present in the HS states, by avoiding the formation of a stable superoxo adduct.

The formation of the LS and HS states of [Co^{II}(**1**)] was found not to be exclusively limited to acetic acid. Similar changes in spin states were also observed using other mild organic acids, including benzoic acid and propanoic acid (Figure 3). It should be noted that the acid dissociation constants (K_a's) for the three acids used in this work are small (pK_a's in H_2O: HOBz, 4.21; HOAc, 4.79; HOPr, 4.87); thus, even in a toluene solution the extent of dissociation will be small, so the concentration of the conjugate anions should be low in each case. Nevertheless, the high intensities of the B-type species in Figure 3 suggest that appreciable dissociation must occur to account for these strong signals (presumably as anion coordination by OAc$^-$, OBz$^-$, and OPr$^-$ affects the dissociation equilibrium). Furthermore, since the spectra reported in Figure 3 were recorded under identical experimental conditions, it also appears that formation of the HS Co^{II} complexes is somewhat more preferred with the bulky OBz$^-$ and OPr$^-$ anions compared to OAc$^-$.

Nature of Species C {(AcO$^-$)[Co^{II}(1)···$O_2^-$$Co^{III}$(1)]-(HOAc)}. As seen earlier, exposure of molecular oxygen to the anaerobically activated system resulted in the loss of signals A and B and the concomitant formation of species C, with spectral parameters typical for HS Co^{II} species (Table 1). This process was found to be largely reversible for the acetic acid system. Species C could also be formed by direct activation of [Co^{II}(**1**)] with HOAc under aerobic conditions. A similar broad EPR spectrum was also observed following activation with benzoic acid and propanoic acid, although with lower apparent intensity.

The precise structural identity of species C is not immediately obvious on the basis of only these *g* values, since similar EPR signals can be obtained from a wide variety of HS Co^{II} centers in different symmetries and coordination environments.[59−62] Of particular relevance to the current system are the penta- and hexacoordinated HS Co^{II}−Schiff base complexes.[63,64] Despite the strong ligand field created in these complexes, favoring the LS state, the HS state can also be accessed by perturbing the equatorial ligand field using electron-attracting carboxylic groups on each aromatic ring of the Schiff base (effectively the positions occupied by the outer *tert*-butyl groups in (**1**)).[64] A similar effect was also observed in the octahedral [Co^{II}(EDTA)] complexes bearing coordinated H_2O ligands, where signals typical of HS Co^{II} were detected at low temperatures.[65] Therefore, in addition to the well-known

dx.doi.org/10.1021/ic300058p | Inorg. Chem. 2012, 51, 8014−8024

LS states, discrete penta- or hexacoordinated Co^{II}–salen type complexes can also exist in a HS state, as indeed shown earlier for the five-coordinate HS species B.

One must also consider the role of clustering by [Co(**1**)] complexes in the assignment of species C. Variations in the redox state and nuclearity of cobalt containing Schiff base type complexes can occur in the presence of bridging OAc^- and O_2 groups.[20,21] The phenoxo-oxygen atoms of salen-type ligands can form μ^2-bridges to more than one metal center, and coupled with the presence of bidentate acetate anions, this can result in the formation and stabilization of high nuclearity cobalt–salen complexes.[20,21,66−69] However, it seems highly unlikely that such mixed valence clusters with a net $S = {}^3/_2$ ground state are formed under the current experimental conditions, since these clusters are usually synthesized directly from a solution of $[Co(OAc)_2]$ with an appropriate bi- or tetradentate ligand[68,69] (rather than the current system where the preformed [Co(**1**)] is present and very stable).

Smaller clusters (dimers) have been considered within the context of catalyst deactivation for [Co(**1**)]. A recent ESI-MS study by Jain et al.[14] examined the importance of the counterion reactivity and dimer formation on the deactivation of [Co(**1**)]. While a major peak at m/z of 603.5 was observed (attributed to [Co(**1**)]), a second set of minor peaks in the m/z range 1207–1251 was also identified (attributed to dimer formation).[14] Interestingly, the mass spectrum of a fresh Co–OAc salen complex diluted in dichloromethane for 24 h showed very substantial formation of dimers.[14] However, the conversion and enantioselectivity in the HKR reaction was identical for the fresh and dimerized material, revealing that dimer formation was not responsible for deactivation. Of relevance to the current work, this ESI-MS data reveals that dimeric complexes can clearly form in the activated [Co(**1**)] system. Owing to the large propensity for Co^{II} complexes to reversibly bind molecular oxygen forming peroxo bridged complexes,[51] and in the presence of bidentate bridging acetate anions, such dimeric complexes would not be unexpected in the current anaerobic and aerobic systems.

Crucially, molecular oxygen is required for the formation of species C (Figure 1). Furthermore, since this transformation is reversible under a nitrogen atmosphere (Figure 4), at least for the [Co(**1**)]/acetic acid system, this strongly suggests that species C must contain a labile dioxygen linkage. We therefore tentatively propose a dimeric structure for species C labeled $(AcO^-)[Co^{II}(\mathbf{1})\cdots O_2{}^-Co^{III}(\mathbf{1})](HOAc)$ (Scheme 1 and eq 3). While the final spin state of species C is uncertain, since the coupling of an $S = {}^1/_2$ spin system with the $S = {}^3/_2$ spin state of $[Co(\mathbf{1})](OAc^-)$ could produce a net $S = 1$ or $S = 2$ spin state, nevertheless it is clear from EPR that species C exists in a HS state:

$$[Co^{II}(\mathbf{1})](HOAc)\ (\mathbf{LS}) + O_2 \rightarrow [Co^{III}(\mathbf{1})O_2{}^-](HOAc) + (OAc^-)[Co^{II}(\mathbf{1})]\ (\mathbf{HS})$$
$$\rightarrow (AcO^-)[Co^{II}(\mathbf{1})\cdots O_2{}^-Co^{III}(\mathbf{1})](HOAc) \quad (3)$$

The well-known Co^{III}–superoxo adducts, formed by dioxygen coordination to pentacoordinated Co^{II}–salen complexes,[51] are characterized by a rhombic EPR signal (Table 1). These species were surprisingly not directly observed in Figure 1c, despite the fact that the $|z^2,{}^2A_1\rangle$ ground state of species A should facilitate formation of the superoxo $[Co^{III}(\mathbf{1})O_2{}^-](HOAc)$ adducts. One explanation for this lack of any EPR observable Co^{III}–superoxo signals is that a dimer forms between $[Co^{III}(\mathbf{1})O_2{}^-](HOAc)$ and the HS pentacoordinated $[Co^{II}(\mathbf{1})](OAc^-)$ complex. A similar dimeric superoxo adduct was in fact reported by Niswander and Taylor[70] on the basis of two Co^{II} Schiff base ligands. Their dimeric complex was considered as having two nonequivalent halves, i.e., $[(SALMeDPT)Co^{III}–O_2{}^-\cdots Co^{II}(SALMeDPT)]$ where SALMeDPT = the methyl derivative of bis(salicylideniminato-3-propyl)amine. The unusual magnetic moment of 3.26 μ_B was explained in terms of the magnetic exchange between the Co^{III}-superoxo ligand and the HS Co^{II} complex.[70] The association between these penta- and hexacoordinated complexes was suggested to arise by a dipole–dipole or ion–dipole interaction,[70] producing an EPR spectrum with a profile analogous to that observed here for species C. In the current system, removal of oxygen, by purging with nitrogen, was shown to regenerate species A and B. The reversible binding of dioxygen in the Co^{III}–superoxo adducts would thus regenerate species A, and simultaneously release the HS pentacoordinated complex back into solution, thereby accounting for the re-emergence of species B. Interestingly, the HS ground state in species B probably prevents formation of a superoxo adduct under aerobic conditions, and this enables a direct transformation of species B to the active $[Co^{III}(\mathbf{1})](OAc^-)$ species without the formation of an intermediary and stable superoxo adduct.

As mentioned earlier, dimer formation can readily occur in [Co(**1**)] complexes, and furthermore, dimeric species were shown not to be detrimental to the HKR catalytic reaction.[14] Therefore, although a large fraction of the $[Co^{II}(\mathbf{1})]$ complexes are converted to diamagnetic species (such as $[Co^{III}(\mathbf{1})](OAc^-)$ for example) following *aerobic* activation with acetic acid, some residual paramagnetic centers in the form of species C $(AcO^-)[Co^{II}(\mathbf{1})\cdots O_2{}^-Co^{III}(\mathbf{1})](HOAc)$ remain. Indeed, the actual [Co(**1**)]-based HKR catalyst can be regenerated several times, with no loss in activity, simply by stirring [Co(**1**)] in acetic acid under aerobic conditions, and as reported by Jain et al.,[14] the dimers are not responsible for any loss in activity. It is not clear why the reversibility summarized in Scheme 1 was only observed using acetic acid (purging the benzoic acid and propanoic acid activated system with nitrogen did not lead to regeneration of species A and B), and we are currently investigating this further.

Nature of the Diamagnetic Species. Following the activation of the $[Co^{II}(\mathbf{1})]$ complex with acetic acid under aerobic conditions, the formation of diamagnetic centers occurs, as indicated by UV–vis data and the observed changes in EPR signal intensity. Earlier studies have identified the presence of Co^{III} complexes that are believed to be the active species.[11] In view of the above discussion, that the C-type complex is due to the linking of A- and B-type complexes by dioxygen (leading to formation of the HS dimer $(AcO^-)[Co^{II}(\mathbf{1})\cdots O_2{}^-Co^{III}(\mathbf{1})](HOAc)$), it is very probable that the more common type of diamagnetic *peroxo* bridged cobalt dimers are also formed in the presence of molecular oxygen. In other words, there is formation of EPR silent $(HOAc)[Co^{III}(\mathbf{1})(O_2{}^{2-})Co^{III}(\mathbf{1})](HOAc)$ dimers possessing a peroxo linkage which are formed between two LS A-type complexes. The observation of the EPR features of the well recognized Co^{III}–superoxo adducts ($[Co^{III}(\mathbf{1})O_2{}^-]$, species E) after induced thermal decomposition at 70 °C followed by rapid freeze-quenching (Figure 4d) corroborates this suggestion, and the Co^{III}–superoxo species can be accounted for by the thermal

dx.doi.org/10.1021/ic300058p | Inorg. Chem. 2012, 51, 8014–8024

breaking of either the *peroxo*-bridged diamagnetic dimers or the *superoxo*-bridged species C.

The current results clearly show the interplay between Co^{II}/Co^{III} redox states while demonstrating the complexity of the [Co(**1**)] system following acetic acid activation. In this respect, it is important to remark that Jacobsen described in early work how [Co^{III}(**1**)](OAc$^-$) catalysts are sometimes reduced to Co^{II} after reaction, and how these can be regenerated by an oxidative treatment using acetic acid.[11]

CONCLUSIONS

The Co(salen) type complex [Co^{II}(**1**)] is an extremely successful homogeneous catalyst for the hydrolytic kinetic resolution (HKR) of epoxides, once it is appropriately activated with a weak organic acid, such as acetic acid under air. Following this treatment, the diamagnetic [Co^{III}(**1**)](OAc$^-$) species is considered to be the active component of the HKR catalyst. Here we have used EPR, HYSCORE, and DFT to examine the nature of the unusual and unexpected HS complexes formed during this activation process. Under *anaerobic* conditions, acetic acid addition to a toluene solution of [Co(**1**)] leads to the expected formation of a LS [Co^{II}(**1**)](HOAc) complex with a $|z^2, {}^2A_1\rangle$ ground state (species A). In addition an unexpected HS [Co^{II}(**1**)](OAc$^-$) complex (species B) is also formed. An analogous set of LS and HS complexes was also identified with benzoic/propanoic acid. The existence of the LS and HS states, induced by coordination of the acid or base, was confirmed using DFT. By comparison, under *aerobic* conditions an unusual paramagnetic HS cobalt-based complex is also generated (species C); this species has been formulated as the superoxo-bridged dimer (AcO$^-$)-[Co^{II}(**1**)$\cdots O_2^-$$Co^{III}$(**1**)](HOAc). Regeneration of the Co^{II} species A and B was achieved simply by removal of O_2 from the solution; this reversibility was not, however, observed with benzoic or propanoic acid. Thermal annealing experiments also revealed the presence of the superoxo [Co^{III}(**1**)O_2^-](HOAc) adducts (species E), originating from the break-up of species C and/or the more common diamagnetic peroxo-bridged dimers (HOAc)[Co^{III}(**1**)(O_2^{2-})Co^{III}(**1**)](HOAc).

Overall, it appears that a facile interconversion of the [Co(**1**)] complex, possessing a LS $|yz, {}^2A_2\rangle$ ground state, occurs in the presence of acetic acid, producing both HS and LS Co^{II} states, prior to formation of the oxidized active form of the catalyst, [Co^{III}(**1**)](OAc$^-$). The HS [Co^{II}(**1**)](OAc$^-$) complex does not enable the stabilization of a superoxo complex in the presence of oxygen. Furthermore, addition of dioxygen results in the formation of a paramagnetic dimer, where the high-spin Co^{II} complex is associated with the oxygenated low spin state (formally a $Co^{II}-O_2^-Co^{III}$ complex). This contrasts with the well-known diamagnetic dimers that are formed when dioxygen links two low-spin Co^{II} Schiff base states giving rise to an effective $Co^{III}-O_2^{2-}-Co^{III}$ complex.

ASSOCIATED CONTENT

Supporting Information

Additional figures, table, and details. This material is available free of charge via the Internet at http://pubs.acs.org.

AUTHOR INFORMATION

Corresponding Author

*E-mail: Sabine.VanDoorslaer@ua.ac.be (S.V.D.), MurphyDM@cardiff.ac.uk (D.M.M.).

Notes

The authors declare no competing financial interest.

ACKNOWLEDGMENTS

The research was supported by the Fund of Scientific Research-Flanders (FWO) (Project G.0312.05N to S.V.D.). S.V.D also is thankful for the support of the Hercules Foundation, Flanders (Contract AUHA013). Funding from the U.K. research council EPSRC (EP/E030122, EP/H023879) is gratefully acknowledged.

REFERENCES

(1) Berrisford, D. J.; Bolm, C.; Sharpless, K. B. *Angew. Chem., Int. Ed.* **1995**, *34*, 1059−1070.
(2) Walsh, P. J.; Kozlowski, M. C. *Fundamentals of Asymmetric Catalysis*; University Science Books: Sausalito, CA, 2009.
(3) Movassaghi, M.; Jacobsen, E. N. *Science* **2002**, *298*, 1904−1905.
(4) *Organometallics in Process Chemistry*; Larsen, R., Ed.; Springer: Berlin, 2004; p 6.
(5) Zhang, W.; Loebach, J. L.; Wilson, S. R.; Jacobsen, E. N. *J. Am. Chem. Soc.* **1990**, *112*, 2801−2803.
(6) Tokunaga, M.; Larrow, J. F.; Kakiuchi, F.; Jacobsen, E. N. *Science* **1997**, *277*, 936−938.
(7) Kim, G. J.; Lee, H.; Kim, S. J. *Tetrahedron Lett.* **2003**, *44*, 5005−5008.
(8) Jacobsen, E. N. *Acc. Chem. Res.* **2000**, *33*, 421−431.
(9) Nielsen, L. P. C.; Stevenson, C. P.; Blackmond, D. G.; Jacobsen, E. N. *J. Am. Chem. Soc.* **2004**, *126*, 1360−1362.
(10) Kemper, S.; Hrobarik, P.; Kaupp, M.; Schlorer, N. E. *J. Am. Chem. Soc.* **2009**, *131*, 4172−4173.
(11) White, D. E.; Jacobsen, E. N. *Tetrahedron: Asymmetry* **2003**, *14*, 3633−3638.
(12) Furrow, M. E.; Schaus, S. E.; Jacobsen, E. N. *J. Org. Chem.* **1998**, *63*, 6776−6777.
(13) Jain, S.; Venkatasubbaiah, K.; Jones, C. W.; Davis, R. J. *J. Mol. Catal. A: Chem.* **2010**, *316*, 8−15.
(14) Jain, S.; Zheng, X.; Jones, C. W.; Weck, M.; Davis, R. J. *Inorg. Chem.* **2007**, *46*, 8887−8896.
(15) Kim, G. J.; Park, D. W. *Catal. Today* **2000**, *63*, 537−547.
(16) Kwon, M. A.; Kim, G. J. *Catal. Today* **2003**, *87*, 145−151.
(17) Gill, C. S.; Venkatasubbaiah, K.; Phan, N. T. S.; Weck, M.; Jones, C. W. *Chem.—Eur. J.* **2008**, *14*, 7306−7313.
(18) Welby, J.; Rusere, L. N.; Tanski, J. M.; Tyler, L. A. *Inorg. Chim. Acta* **2009**, *362*, 1405−1411.
(19) Rusere, L. N.; Shalumova, T.; Tanski, J. M.; Tyler, L. A. *Polyhedron* **2009**, *28*, 3804−3810.
(20) You, Z.-L.; Zhou, P. *Inorg. Chem. Commun.* **2007**, *10*, 1273−1275.
(21) Dong, W.-K.; Duan, J.-G.; Chai, L.-Q.; Liu, G. L.; Wu, H. L. *J. Coord. Chem.* **2008**, *61*, 1306−1315.
(22) Vinck, E.; Van Doorslaer, S.; Murphy, D. M.; Fallis, I. A. *Chem. Phys. Lett.* **2008**, *464*, 31−37.
(23) Vinck, E.; Murphy, D. M.; Fallis, I. A.; Strevens, R. R.; Van Doorslaer, S. *Inorg. Chem.* **2010**, *49*, 2083−2092.
(24) Stoll, S.; Schweiger, A. *J. Magn. Reson.* **2006**, *178*, 42−55.
(25) Höfer, P.; Grupp, A.; Nebenführ, H.; Mehring, M. *Chem. Phys. Lett.* **1986**, *132*, 279−282.
(26) Smith, S. A.; Levante, T. O.; Meier, B. H.; Ernst, R. R. *J. Magn. Reson.* **1994**, *106*, 75−105.
(27) Madi, Z. L.; Van Doorslaer, S.; Schweiger, A. *J. Magn. Reson.* **2002**, *154*, 181−191.
(28) Neese, F. *J. Chem. Phys.* **2001**, *115*, 11080−11096.
(29) Neese, F. *J. Phys. Chem. A* **2001**, *105*, 4290−4299.
(30) Neese, F. *J. Chem. Phys.* **2003**, *118*, 3939−3948.
(31) Neese, F. *J. Chem. Phys.* **2005**, *122*, 34107(1)−34107(13).
(32) Schäfer, A.; Horn, H.; Ahlrichs, R. *J. Chem. Phys.* **1992**, *97*, 2571−2577.
(33) Dill, J. D.; Pople, J. A. *J. Chem. Phys.* **1975**, *62*, 2921−2923.

(34) Hehre, W. J.; Ditchfie., R.; Pople, J. A. *J. Chem. Phys.* **1972**, *56*, 2257−2261.
(35) Krishnan, R.; Binkley, J. S.; Seeger, R.; Pople, J. A. *J. Chem. Phys.* **1980**, *72*, 650−654.
(36) Barone, V. In *Recent Advances in Density Functional Methods*; Chong, D. P., Ed.; World Scientific.: Singapore, 1996; p 287.
(37) Sinnecker, S.; Rajendran, A.; Klamt, A.; Diedenhofen, M.; Neese, F. *J. Phys. Chem. A* **2006**, *110*, 2235−2245.
(38) Reynolds, J. A.; Hough, J. M. *Proc. Phys. Soc., London, Sect. B* **1957**, *70*, 769−775.
(39) Perdew, J. P. *Phys. Rev. B* **1986**, *33*, 8822−8824.
(40) Perdew, J. P. *Phys. Rev. B* **1986**, *34*, 7406−7406.
(41) Becke, A. D. *Phys. Rev. A* **1988**, *38*, 3098−3100.
(42) Dunlap, B. I.; Connolly, J. W. D.; Sabin, J. R. *J. Chem. Phys.* **1979**, *71*, 3396−3402.
(43) Vahtras, O.; Almlöf, J.; Feyereisen, M. W. *Chem. Phys. Lett.* **1993**, *213*, 514−518.
(44) Pietrzyk, P.; Srebro, M.; Radón, M.; Sojka, Z.; Michalak, A. *J. Phys. Chem. A* **2011**, *115*, 2316−2324.
(45) Daul, C.; Schläpfer, C. W.; von Zelewsky, A. *Struct. Bonding (Berlin)* **1979**, *36*, 129−171.
(46) Hurst, G. C.; Henderson, T. A.; Kreilick, R. W. *J. Am. Chem. Soc.* **1985**, *107*, 7294−7299.
(47) Schaus, S. E.; Brandes, B. D.; Larrow, J. F.; Tokunaga, M.; Hansen, K. B.; Gould, A. E.; Furrow, M. E.; Jacobsen, E. N. *J. Am. Chem. Soc.* **2002**, *124*, 1307−1315.
(48) Walker, F. A. *J. Am. Chem. Soc.* **1970**, *92*, 4235−4244.
(49) Swart, M.; Güell, M.; Solà, M. In *Quantum Biochemistry*; Matta, C. F., Ed.; Wiley-VCH: Weinheim, 2010; Chapter 19, p 551.
(50) Neese, F. *Coord. Chem. Rev.* **2009**, *253*, 526−563.
(51) Cotton, F. A.; Wilkinson, G.; Bochmann, M.; Grimes, R. N. *Advanced Inorganic Chemistry*, 5th ed.; Wiley Interscience Publications: New York, 1999.
(52) Bolzacchini, E.; Canevali, C.; Morazzoni, F.; Orlandi, M.; Rindone, B.; Scotti, R. *J. Chem. Soc., Dalton Trans.* **1997**, 4695−4699.
(53) Valentin, J. S. *Chem. Rev.* **1973**, *73*, 235−245.
(54) Van Doorslaer, S.; Schweiger, A.; Krautler, B. *J. Phys. Chem. B* **2001**, *105*, 7554−7563.
(55) Bowen, J. H.; Shokhirev, N. V.; Raitsimring, A. M.; Buttlaire, D. H.; Walker, F. A. *J. Phys. Chem. B* **1997**, *101*, 8683−8691.
(56) Walker, F. A. *J. Magn. Reson.* **1974**, *15*, 201−218.
(57) Walker, F. A. *J. Am. Chem. Soc.* **1973**, *95*, 1154−1159.
(58) Hoffman, B. M.; Szymanski, T.; Basolo, F. J. *Am. Chem. Soc.* **1975**, *97*, 673−674.
(59) Bianchini, C.; Gatteschi, D.; Giambastiani, G.; Rios, I. G.; Ienco, A.; Laschi, F.; Mealli, C.; Meli, A.; Sorace, L.; Toti, A.; Vizza, F. *Organometallics* **2007**, *26*, 726−739.
(60) Pilbrow, J. R. In *Transition Ion Electron Paramagnetic Resonance*; Oxford Science Publications: Oxford, U.K., 1990.
(61) Bencini, A.; Beni, A.; Costantino, F.; Dei, A.; Gatteschi, D.; Sorace, L. *Dalton Trans.* **2006**, 722−729.
(62) Carlin, R. L.; O'Connor, C. J.; Bhatia, S. N. *J. Am. Chem. Soc.* **1976**, *98*, 685−688.
(63) Boca, R.; Elia, H.; Haase, W.; Huber, M.; Klement, R.; Muller, L.; Paulus, H.; Svoboda, I.; Valko, M. *Inorg. Chim. Acta* **1998**, *278*, 127−135.
(64) Thuery, P.; Zarembowitch, J. *Inorg. Chem.* **1986**, *25*, 2001−2008.
(65) Kang, P. C.; Eaton, G. R.; Eaton, S. S. *Inorg. Chem.* **1994**, *33*, 3660−3665.
(66) Chun, Y.; Wang, Q. L.; Tang, G. T.; Chao, W.; Yan, S. P.; Liao, D. Z. *J. Coord. Chem.* **2010**, *63*, 505−514.
(67) Mechi, L.; Siega, P.; Dreos, R.; Zangrando, E.; Randaccio, L. *Eur. J. Inorg. Chem.* **2009**, 2629−2638.
(68) Chattopadhyay, S.; Bocelli, G.; Musatti, A.; Ghosh, A. *Inorg. Chem. Commun.* **2006**, *9*, 1053−1057.
(69) Chattopadhyay, S.; Drew, M. G. B.; Ghosh, A. *Eur. J. Inorg. Chem.* **2008**, 1693−1701.
(70) Niswander, R. H.; Taylor, L. T. *J. Am. Chem. Soc.* **1977**, *99*, 5935−5939.
(71) Jorin, E.; Rudin, M.; Schweiger, A.; Gunthard, H. H. *Chem. Phys. Lett.* **1980**, *69*, 193−197.
(72) Lubitz, W.; Winscom, C. J.; Diegruber, H.; Moseler, R. *Z. Naturforsch., A: Phys. Sci.* **1987**, *42*, 970−986.
(73) Van Doorslaer, S.; Jeschke, G.; Epel, B.; Goldfarb, D.; Eichel, R. A.; Krautler, B.; Schweiger, A. *J. Am. Chem. Soc.* **2003**, *125*, 5915−5927.